Magnetic structure, excitations, and field-induced transitions in the honeycomb lattice compound $Er_2Si_2O_7$

M. Islam,[1,*] N. d'Ambrumenil,[1] D. D. Khalyavin,[2] P. Manuel,[2] F. Orlandi,[2] J. Ollivier,[3] M. Ciomaga Hatnean,[1,†] G. Balakrishnan,[1] and O. A. Petrenko[1,‡]

[1]*Department of Physics, University of Warwick, Coventry CV4 7AL, United Kingdom*
[2]*ISIS Facility, STFC Rutherford Appleton Laboratory, Chilton, Didcot OX11 0QX, United Kingdom*
[3]*Institut Laue-Langevin, 71 Avenue des Martyrs, CS 20156, 38042 Grenoble Cedex 9, France*

(Received 9 October 2023; revised 23 January 2024; accepted 15 February 2024; published 14 March 2024)

We investigate the magnetic properties of the monoclinic D-type $Er_2Si_2O_7$ with a distorted honeycomb lattice using powder and single-crystal neutron scattering techniques, as well as single-crystal magnetization measurements. The powder neutron diffraction shows that below the ordering temperature, $T_N = 1.85$ K, the compound forms a $\mathbf{q} = \mathbf{0}$ antiferromagnetic structure with four sublattices. For $H \parallel a$, magnetization measurements reveal a narrow but clearly visible plateau at one-third of the magnetization saturation value. The plateau's stabilization is accompanied by a significant increase of the magnetic unit cell, as the magnetic peaks with fractional indices are observed in single-crystal neutron diffraction experiments. At low temperatures, the inelastic neutron scattering measurements reveal the presence of low-energy, almost dispersionless excitations. Their spectrum is sensitive to the applied field, it significantly softens on the magnetization plateau, and demonstrates the behavior expected for a noncollinear Ising antiferromagnet away from the plateau.

DOI: 10.1103/PhysRevB.109.094420

I. INTRODUCTION

The family of rare-earth (R) disilicates $R_2Si_2O_7$ is renowned for its complex polymorphism with at least seven different crystal structures possible depending on the particular rare-earth ion, temperature range, and pressure during synthesis [1–3]. There is a significant volume of experimental work on their structural phase transitions, sample preparation, and characterization, as well as single-crystal growth, but surprisingly little is known about the magnetic properties of these compounds. In several of the polymorphic crystal structures, the magnetic R ions are arranged into a (distorted) honeycomb lattice, which makes them potentially very interesting from the contemporary magnetism point of view, particularly when searching for the experimental realizations of the Kitaev model [4]. Despite a large moment typically associated with the R ions, the magnetic behavior of $R_2Si_2O_7$ disilicates is not necessarily classical, as $Yb_2Si_2O_7$, for example, is considered to be a strongly spin-orbit-coupled quantum dimer magnet [5].

Erbium disilicate, $Er_2Si_2O_7$, can be formed in three polymorphs, a triclinic $P\bar{1}$ low-temperature phase (labeled as B-type), a monoclinic $C2/m$ phase (C-type) [6], and a high-temperature monoclinic $P2_1/b$ phase (D-type). Here we report on the magnetic properties of the monoclinic D-type phase (see Fig. 1), for which large, high-quality single-crystal samples are available [7] and focus on its rather unusual in-field behavior. The initial magnetic properties studies reported by Leask *et al.* [8] on the D-phase of $Er_2Si_2O_7$ suggested a four-sublattice antiferromagnetic ground state below the ordering temperature of 1.9 K. This hypothesis has recently received a direct experimental confirmation from powder neutron diffraction (PND) measurements [9]. A pronounced Ising-like character of $Er_2Si_2O_7$ is evident from the highly anisotropic magnetization curves, which were (at least partially) understood within a fairly simple model backed up by Monte Carlo simulations [8]. However, one experimental observation, a stabilization of the $\frac{1}{3}$ magnetization plateau for a field applied along the a axis, was at odds with the theoretical predictions for a model with four sublattices in the magnetic unit cell. A possibility of the enlarged magnetic unit cell was briefly mentioned, but dismissed as unlikely [8]. We find that in the narrow region of applied magnetic fields corresponding to the $\frac{1}{3}$ magnetization plateau, the magnetic unit cell is indeed increased severalfold, as witnessed by a spectacular transformation of the single-crystal neutron diffraction patterns.

The appearance of the $\frac{1}{3}$ magnetization plateaus in triangular lattice antiferromagnets, quantum and classical, is a common feature, and is often associated with the stabilization of the *up-up-down* (uud) structures in Heisenberg, XY, and Ising systems by various mechanisms. In the case of only nearest-neighbor (NN) interactions, the honeycomb

*manisha.islam@warwick.ac.uk
†Present addresses: Materials Discovery Laboratory, Department of Materials, ETH Zurich, 8093 Zurich and Laboratory for Multiscale materials eXperiments, Paul Scherrer Institute (PSI), 5232 Villigen, Switzerland.
‡o.petrenko@warwick.ac.uk

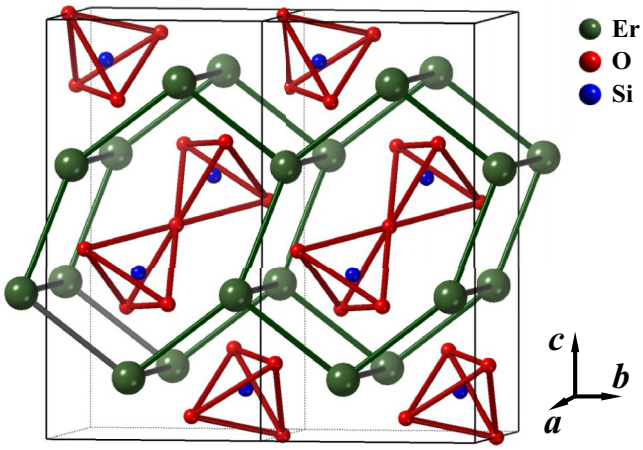

FIG. 1. Crystal structure of the monoclinic D-type $Er_2Si_2O_7$ (space group $P2_1/b$). The bonds between the magnetic Er^{3+} ions emphasize the formation of the distorted honeycomb layers stacked along the a axis. The unit cells are shown in black.

structure is bipartite and not frustrated, however the next NN interactions could drive it towards a frustrated regime with an extensive ground-state degeneracy. The resulting behavior is then typical for highly frustrated magnets with complex and fragile ground states sensitive to minute perturbations. In many cases, the symmetry breaking by an external magnetic field is not trivial, and the fractional magnetization plateaus are expected. Recent reports suggest, for example, stabilization of the $\frac{1}{3}$ and $\frac{2}{3}$ magnetization plateaus in a quantum antiferromagnet $Cu_2(pymca)_3(ClO_4)$ on a distorted honeycomb lattice [10,11]. For another two-dimensional honeycomb system, $DyNi_3Ga_9$, the plateaus are found for every $\frac{1}{6}$ of the saturation value [12]. A theoretical study [13] suggests the stabilization of the $\frac{1}{3}$ and $\frac{2}{3}$ plateaus in the XY model with third NN interactions on the honeycomb lattice through the order-by-disorder mechanism. In this paper, we explore the complex magnetization process in the distorted honeycomb lattice antiferromagnet $Er_2Si_2O_7$ with four noncollinear Ising-like classical spins in the unit cell.

II. EXPERIMENTAL PROCEDURES

An $Er_2Si_2O_7$ crystal boule was prepared by the floating zone method using a two-mirror halogen lamp optical image furnace (NEC SC1MDH-11020, Canon Machinery Incorporated). The growth was performed in air, at ambient pressure and at a growth speed of 12 mm/h. The crystal growth of $Er_2Si_2O_7$ is described elsewhere in a more detailed paper [7]. Phase purity analysis was carried out on a ground crystal piece of $Er_2Si_2O_7$, and the room-temperature powder x-ray diffraction on Pananalytical and Bruker diffractometers using Cu $K\alpha_1$ and Cu $K\alpha_2$ ($\lambda_{K\alpha1} = 1.5406$ Å and $\lambda_{K\alpha2} = 1.5444$ Å) radiation confirms that the crystallographic structure of the crystal boule is D-type.

As previously reported [7,14], the conventional synthesis by the solid-state method of polycrystalline samples of D-type $Er_2Si_2O_7$ results in the presence of a small amount of an Er_2SiO_5 impurity. To ensure the purity of the $Er_2Si_2O_7$ powder specimen used in our experiments, a polycrystalline sample ($\approx$2g) was prepared by crushing a fragment of the crystal boule. Room-temperature powder x-ray diffraction measurements confirmed that there was no evidence of the presence of the $Er_2Si_2O_5$ or any other phase impurity in the crushed crystal boule. The measurements described here were all taken on samples isolated from this single-crystal boule.

We used a Quantum Design MPMS SQuID magnetometer for the magnetization measurements in applied magnetic fields of up to 70 kOe. An iQuantum ^{3}He insert [15] allowed the temperature range explored to be extended down to 0.48 K. To estimate the demagnetization factors, we used a rectangular prism approximation [16].

The WISH time-of-flight diffractometer [17] at the ISIS facility at the Rutherford Appleton Laboratory (STFC, UK) was used for both the powder (PND) and single-crystal neutron diffraction experiments [18]. A ^{3}He absorption refrigerator provided a base temperature of 0.24 K for neutron diffraction measurements. For PND, the data obtained at $T = 10$ K were used as a background to isolate the magnetic signal for each temperature. Rietveld refinements were performed using the FULLPROF software suite [19]. For the single-crystal diffraction measurements, a sample of mass 250 mg was aligned with its a axis vertical (parallel to the applied field) for access to the reflections within $\pm$7.5 degrees of the horizontal b^*-c^* scattering plane.

The inelastic neutron scattering (INS) measurements [20] were performed on the time-of-flight spectrometer IN5 [21] at the Institut Laue-Langevin (ILL), Grenoble, France on sample of mass 475 mg. An incident wavelength of $\lambda = 4.8$ Å ($E_i = 3.55$meV) with an elastic resolution of $\delta E \simeq 86\,\mu$eV full width at half-maximum has been chosen throughout the measurements. For each field and temperature condition, scans between 4 and 10 min have been recorded every 1° crystal rotation. Data have been reduced under MANTID [22] and analyzed with the Horace [23] library under MATLAB.

III. RESULTS AND DISCUSSION

A. Powder neutron diffraction

Figure 2(a) shows the development of the magnetic correlations in $Er_2Si_2O_7$ upon cooling from 4.0 K to just above the magnetic ordering temperature. At higher temperatures, the scattering signal is broad, but on approaching $T_N = 1.85$ K it becomes more structured. The results are consistent with the data presented in [9]. At 1.9 K, two intensity maxima are clearly visible at 1.16 and 1.27 Å^{-1}, the positions corresponding to the strongest magnetic peaks appearing below T_N. Figure 2(b) emphasizes the stabilization of the long-range magnetic order below $T_N = 1.85$ K and the absence of further transitions down to at least 0.24 K.

Refinement of the PND data taken on WISH at 10 K confirms the monoclinic $P2_1/b$ crystallographic space group with lattice parameters of $a = 4.6911(3)$ Å, $b = 5.5620(4)$ Å, $c = 10.7990(7)$ Å, $\alpha = 90°$, $\beta = 90°$, $\gamma = 96.0470(4)°$. The magnetic contribution of the data at 0.24 K are shown in Fig. 3(a), after the subtraction of the 10 K measurement in the paramagnetic phase.

Upon the isolation of the magnetic signal, an impurity peak was revealed at 1.07 Å^{-1}. The intensity of this impurity

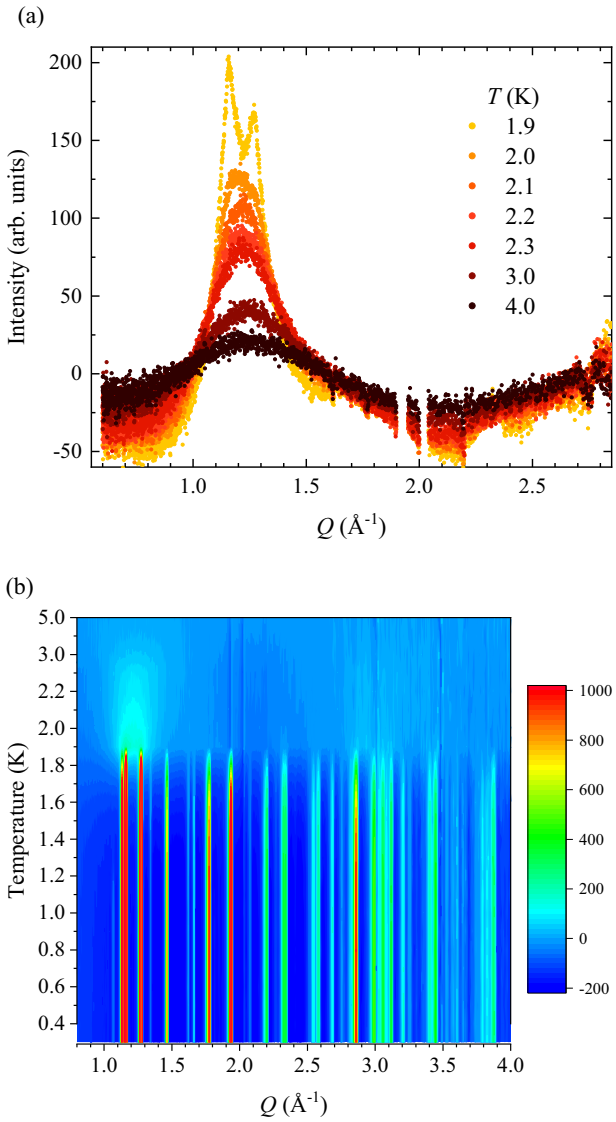

FIG. 2. Temperature evolution of the magnetic neutron diffraction intensity measured on WISH diffractometer [17] using a powder sample of D-type $Er_2Si_2O_7$. Panel (a) shows the development of diffuse signal above ordering temperature. Panel (b) combines all the diffraction data between 0.24 and 5.0 K into an intensity color map. For both panels, the magnetic contribution is obtained by subtracting a 10 K background. The omitted regions in panel (a) correspond to the very strong nuclear Bragg peaks for which the subtraction is imperfect.

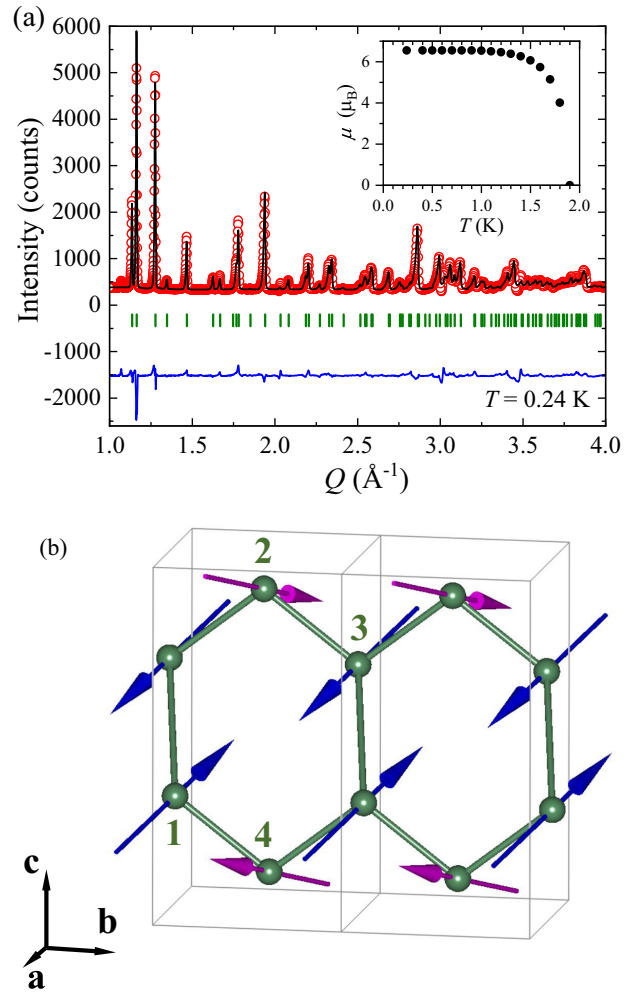

FIG. 3. (a) Rietveld refinement of the PND data in zero field at 0.24 K. The background subtracted data (red circles) from banks 2 and 9 of the WISH diffractometer [17] are shown together with the calculated pattern (black line) and the difference curve (blue line). Green ticks represent the positions of the magnetic Bragg peaks. The inset follows the temperature dependence of the magnitude of the magnetic moment, μ, of the Er^{3+} ions determined by the refinement. (b) Magnetic structure of D-type $Er_2Si_2O_7$ obtained from the PND refinement as viewed along the a axis. Unit cell boundaries are shown in black, with the four constituent magnetic ions labeled from 1 to 4 in green. The positions of the Er^{3+} ions and their moments are listed in Table I.

peak follows a different temperature dependence compared to the main $Er_2Si_2O_7$ phase; it disappears above 1.5 K, which indicates that is it likely to be a magnetic Bragg peak from an impurity phase. As the intensity of this peak is less than 3% of the magnetic signal of the main phase with no indication of the presence of impurity in nuclear structure refinement with PND (as well as with room-temperature PXRD measurements), it can be concluded that only a negligibly small amount of impurity exists in our single-crystal sample.

The presence of magnetic intensities on top of the nuclear Bragg peaks indicates $\mathbf{q} = \mathbf{0}$ propagation vector. The magnetic structure solution was approached based on the space group representation (irrep) theory [24], assuming an irreducible nature of the magnetic order parameter. We focus on the data collected in the detector banks 2 and 9, with an average diffraction angle of 58°, covering a range of 32°. The chosen banks provide the maximum flux of neutrons at the relevant scattering vectors with the best possible resolution. An incorporation of the data from other banks did not significantly modify the results of the refinement.

Systematic testing of the relevant irreps in the refinement of the diffraction pattern revealed that only mGM2- [25,26] provided good quality fitting ($R_{\text{magnetic}} = 10.9\%$). mGM2- is a one-dimensional irrep entering three times into decomposition of the reducible representation associated with the Er Wyckoff

TABLE I. Ionic positions and magnetic moments of the four Er^{3+} ions, obtained from the refinement of zero-field PND data taken at 0.24 K. The labels $\mu_{a,b,c}$ denote the components of the magnetic moments along unit vectors in the $\boldsymbol{a}$, $\boldsymbol{b}$, and $\boldsymbol{c}$ directions. The moments $\langle \boldsymbol{m}_a \rangle$ and $\langle \boldsymbol{m}_c \rangle$ are the theoretical average moments per ion expected if ions flip to align as far as possible with an applied field in the a and c directions.

	Positions	μ_b			Moment
Ion	$(\boldsymbol{a}, \boldsymbol{b}, \boldsymbol{c})$ basis	μ_a	(μ_B)	μ_c	(μ_B)
1	0.89 0.10 0.35	−5.62(2)	2.10(4)	2.08(3)	6.54(4)
2	0.11 0.40 0.85	−5.62(2)	2.10(4)	−2.08(3)	6.54(4)
3	0.11 0.90 0.65	5.62(2)	−2.10(4)	−2.08(3)	6.54(4)
4	0.89 0.60 0.15	5.62(2)	−2.10(4)	2.08(3)	6.54(4)
$\langle \boldsymbol{m}_a \rangle$		5.62(2)	−2.10(4)	0.00	6.20(4)
$\langle \boldsymbol{m}_c \rangle$		0.00	0.00	2.08(3)	2.08(4)

position 4*e*. The corresponding three basis vectors transform the μ_a, μ_b, and μ_c components of the ordered moment specified in Table I. All three components are nonzero, yielding a noncollinear magnetic structure shown in Fig. 3(b) with a total moment of 6.54(4) Bohr magneton (μ_B) at $T = 0.24$ K. A magnetic structure with the unit cell containing four magnetic ions at inequivalent positions was refined, with all magnetic contributions found only at the nuclear peak positions and corresponding to the propagation vector $\mathbf{q} = \mathbf{0}$. A fit with $R = 22.6\%$, $wR = 21.7\%$, and $R_{\text{Bragg}} = 0.9\%$ was achieved for $T = 0.24$K. The temperature dependence of the magnitude of the moment of the Er^{3+} ions is shown in the inset of Fig. 3(a). The moment remains practically independent of temperature at 6.54 μ_B until 1 K, above which it decreases with temperature and drops to zero at 1.9 K.

Figure 3(b) illustrates the resulting magnetic structure of $Er_2Si_2O_7$ after Rietveld refinement. The magnetic ions, shown in green, present a distorted honeycomb arrangement. The unit cell contains four magnetic Er^{3+} ions, and their positions are labeled in Fig. 3(b). The Er^{3+} moments at positions 1 and 3 (blue arrows) and 2 and 4 (pink arrows) are antiferromagnetically aligned to each other and share an easy magnetization axis. Table I details the positions of the ions and components of the magnetic moments as well as the average moment per ion when the spins are flipped by the applied field. The magnetic structure implies $P2_1'/c$ symmetry with the unit cell related to the paramagnetic structure as $(-1, 0, 0)$, $(0, 0, -1)$, and $(0, -1, 0)$ (see the supplementary mcif file [27] for details).

B. Magnetization measurements

Figure 4(a) summarizes the low-temperature susceptibility measurements in 0.1 and 1.0 kOe along the a axis. The magnetic ordering temperature in low fields is seen as a sharp drop in the susceptibility below $T_N = 1.85$ K. No appreciable difference has been noticed in the susceptibility measured in field-cooled and in zero-field-cooled conditions for the applied fields of 0.1 and 1.0 kOe.

Figures 5 and 6 illustrate the magnetization process in $Er_2Si_2O_7$ for two directions of an applied magnetic field, $H \parallel a$ and $H \parallel c$. For both field directions, a rather sharp increase in magnetization $M(H)$ is observed in relatively weak fields, 5.3 kOe for the field applied along the a axis and 3.3 kOe for the field along the c axis.

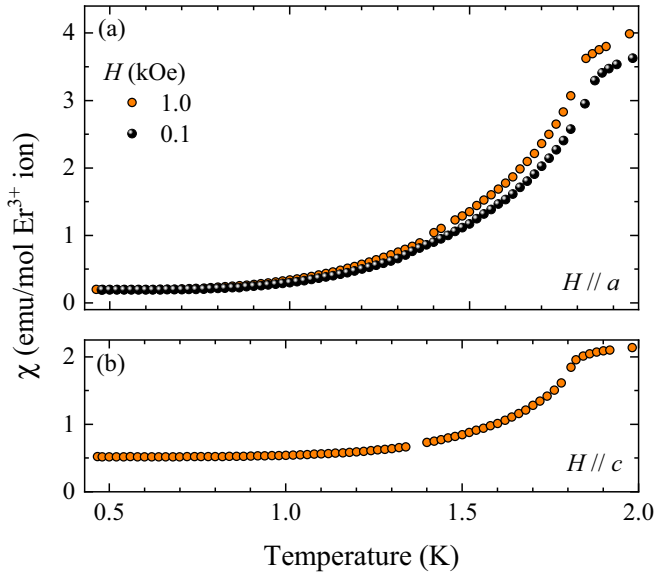

FIG. 4. (a) Temperature dependence of the susceptibility of D-type $Er_2Si_2O_7$ measured in 0.1 and 1.0 kOe for $H \parallel a$. (b) Temperature dependence of the susceptibility measured in 1 kOe for $H \parallel c$. For both field directions, the applied field is quoted without taking into account demagnetization corrections.

For $H \parallel a$, at the lowest temperature, a clear plateau in magnetization is visible, extending from 5.3 to 6.0 kOe. Above the plateau, the $M_{H \parallel a}$ increases again rather sharply, reaching 5.9μ_B per Er^{3+} ion already in a field of 7 kOe and 6.5μ_B in a

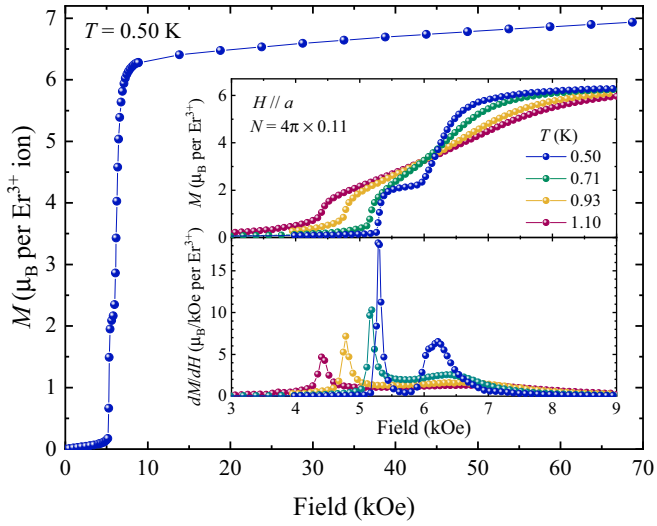

FIG. 5. Field dependence of the magnetization of D-type $Er_2Si_2O_7$ measured at 0.5 K for $H \parallel a$. The inset focuses on the transition found at 5.3 kOe and follows the temperature evolution of (top panel) the magnetization, M, and (bottom panel) its field derivative dM/dH. The applied field is corrected using the demagnetization factor $N_a = 0.11 \times 4\pi$.

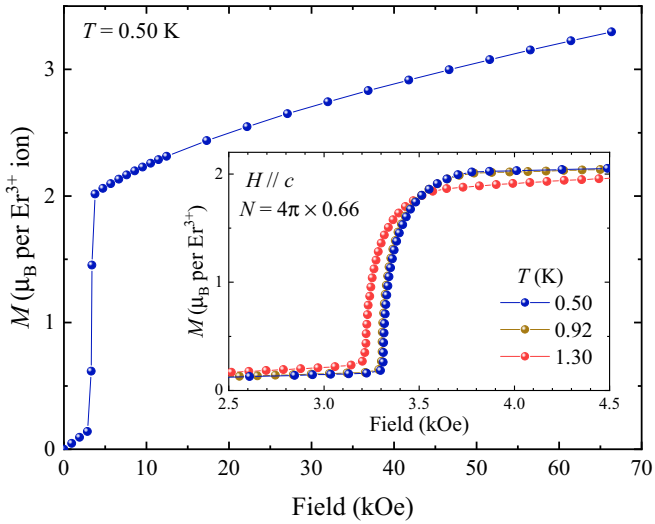

FIG. 6. Field dependence of the magnetization of D-type $Er_2Si_2O_7$ measured at 0.5 K for $H \parallel c$. The inset shows the transition observed at 3.3 kOe on an expanded scale and shows the field dependence of the magnetization around the transition at different temperatures. The applied field is corrected using the demagnetization factor $N_c = 0.66 \times 4\pi$.

field of 20 kOe. This value is in agreement with the total moment of $6.54(4)\mu_B$ obtained from the PND refinements (see Fig. 3). Above 20 kOe, the magnetization tends to saturate with further field increase up to 70 kOe, resulting in a small increase of $M_{H\parallel a}$ to $6.9\mu_B$ per Er^{3+} ion.

The transitions to and from the magnetization plateau are temperature-sensitive (see the inset in Fig. 5) – a minimum in the field derivative dM/dH becomes barely visible at $T = 0.71$ K and disappears completely for $T = 0.93$ and 1.1 K despite the temperature remaining well below the T_N.

For $H \parallel c$, the transition at 3.3 kOe is accompanied by a sudden jump of magnetization from 0.1 to 2.1 μ_B; no signs of a plateau stabilization could be detected for this direction of an applied field (see the inset in Fig. 6). Above the transition field, the $M_{H\parallel c}$ continues to significantly increase reaching 3.3 μ_B per Er^{3+} ion in a maximum field of 70 kOe.

Unlike the case of $H \parallel a$, the magnetization process around the critical field for $H \parallel c$ is not particularly temperature-sensitive.

The magnetization measurement results are in agreement with the previous report [8]. Small variations in the values of the observed critical fields are most likely caused by the uncertainty in the estimates of the demagnetization factor, as the sample used was not a perfect rectangular prism. The estimates of the demagnetization factor of the sample used in magnetization measurements for $H \parallel a$ and $H \parallel c$ are 0.11 and 0.66 (in units of 4π), respectively [16]. Given a relatively high density of $Er_2Si_2O_7$ and large magnetic moments of Er^{3+} ions, the demagnetization field corrections make an appreciable impact on the values of the transition fields.

C. Single-crystal neutron diffraction

We followed the magnetization process in $Er_2Si_2O_7$ for a field applied along the a axis by performing single-crystal neutron diffraction measurements on the WISH diffractometer at ISIS [17]. Above and below the magnetization plateau region, the observed magnetic pattern consists of the $\mathbf{q} = \mathbf{0}$ peaks, while on the plateau, an additional signal around the noninteger $(0kl)$ positions becomes clearly visible (see Fig. 7). The magnetic signal consists of a mixture of the resolution-limited Bragg peaks and much broader diffuse scattering features. There are sharp peaks around the positions described with the propagation vector $\mathbf{q} = (0\frac{1}{2}\frac{1}{2})$ at 6 kOe. The intensity profiles of these peaks become broader along the c^* direction in 7 kOe. In 8 kOe the signal could be described as a collection of diffuse scattering rods with undulating intensity running along the c^* direction at $\frac{1}{2}$-integer values of k. Upon further increase of the applied field to 9 kOe, the intensities of these rods decrease and they almost disappear at 10 kOe.

The phase at 6 kOe, which we associate with the magnetization plateau regime, is also characterized by the appearance of the relatively weak resolution-limited peaks at the $\mathbf{q} = (0\frac{1}{4}\frac{1}{4})$ positions. These peaks are barely visible at 7 kOe and absent in data taken at the other fields. The diffraction pattern in 6 kOe is also characterized by the presence of broad diffuse features elongated along the b^* direction at the $\mathbf{q} = (0\frac{1}{3}0)$ positions, which form the undulating intensity rods running along the b^* axis. These rods are also present in 7 kOe, but in 8 kOe they are transformed into a collection of weak and narrow peaks at $\mathbf{q} = (0\frac{1}{3}0)$ positions.

The additional noninteger diffuse features appear as sharp peaks with intensities comparable to the main magnetic reflections at the $\mathbf{q} = \mathbf{0}$ positions. We have therefore chosen an appropriate scale (2% of the intensity of the Bragg reflections at the $\mathbf{q} = \mathbf{0}$ positions) to best illustrate the weaker diffuse signal within the plateau regime in Figs. 7 and 8. At applied fields of 8 and 9 kOe, the undulating diffuse features appear to tilt along k while traversing along l. The direction of the tilt alternates as the Brillouin zone boundaries are crossed with increasing l. A similar undulation of diffuse scattering rods has previously been linked to the presence of an incommensurate state in the honeycomb systems $SrHo_2O_4$ and $SrEr_2O_4$ [28,29].

The rather irregular shape of the sample, a result of natural cleaving of the as-grown boule, used in the diffraction experiments means that we cannot accurately calculate the demagnetizing factor N, and a comparison between the neutron diffraction and magnetization features is not straightforward. However, just for estimation purposes, if we were to assume that $N_a \approx 0.22 \times 4\pi$, then on a plateau the demagnetizing field is around 12% of the applied field (further discussion is given in Sec. IV). Therefore, for the single-crystal diffraction measurements, an applied field of 6 kOe corresponds to the left-hand side of the magnetization plateau, the field of 7 kOe is very close to its right-hand side, while 8 kOe corresponds to the region of a rapid magnetization growth above the plateau. The fields of 9 and 10 kOe would then correspond to a nearly saturated phase.

Figure 8 compares the magnetic correlations in identical applied fields along the a axis at before (top) and after exposure to a significantly higher field of 50 kOe (bottom). At all fields within the plateau boundaries, there is an apparent asymmetry when looking at the diffuse scattering patterns

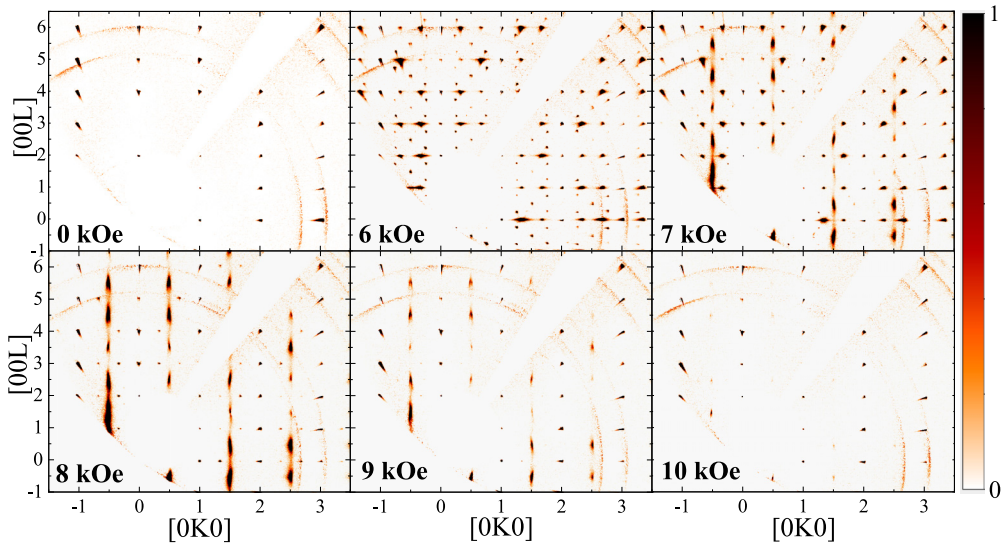

FIG. 7. Magnetic single-crystal neutron diffraction maps of the $(0kl)$ plane for D-type $Er_2Si_2O_7$ measured on the WISH diffractometer at $T = 0.24$ K in different fields applied along the a axis. The magnetic signal is obtained by subtracting the $T = 2$ K background. Only sharp Bragg peaks with integer k and l indices are observed in zero field and in applied fields above 10 kOe (see [27]). The scattering patterns in the fields corresponding to the magnetization plateau are dominated by the appearance of the peaks and diffuse scattering features at fractional positions in reciprocal space.

in Fig. 8. The difference is most pronounced along b^* when comparing the diffuse features at $\mathbf{q} = (0\frac{1}{3}0)$ and $(0\frac{2}{3}0)$. The signal at $(0\frac{2}{3}0)$ is a distinct, sharp Bragg peaklike feature, while at $(0\frac{1}{3}0)$ there is a relatively large diffuse scattering feature elongated along b^*. The diffuse scattering signals on the upward and downward field sweep also differ, with well-defined, diagonal lines of intensity traversing through the $\mathbf{q} = (0\frac{1}{3}0)$ and the surrounding $(0\frac{1}{4}\frac{1}{4})$ peaks appearing on the downward sweep. The resulting starlike shapes are much more pronounced in the patterns taken after the sample was subjected to a high applied field, above the saturation field.

A full set of the diffraction maps measured on WISH can be found in the Supplemental Material [27].

D. Inelastic neutron scattering

The measurements of the excitations performed on the IN5 spectrometer at ILL with a single-crystal sample of $Er_2Si_2O_7$ were taken with the vertical magnetic field applied along the a axis. The measurements of the elastic signal in the b^*-c^* scattering plane allowed for an identification of the magnetic state, as a direct comparison with the magnetization data is again complicated by the irregular sample shape and the associated uncertainty of the demagnetizing factor. We therefore accompany the INS data with the maps of the elastic intensity observed in the b^*-c^* plane. Whenever possible, the diffraction intensity maps have been folded according to the crystal symmetries in order to improve the statistics.

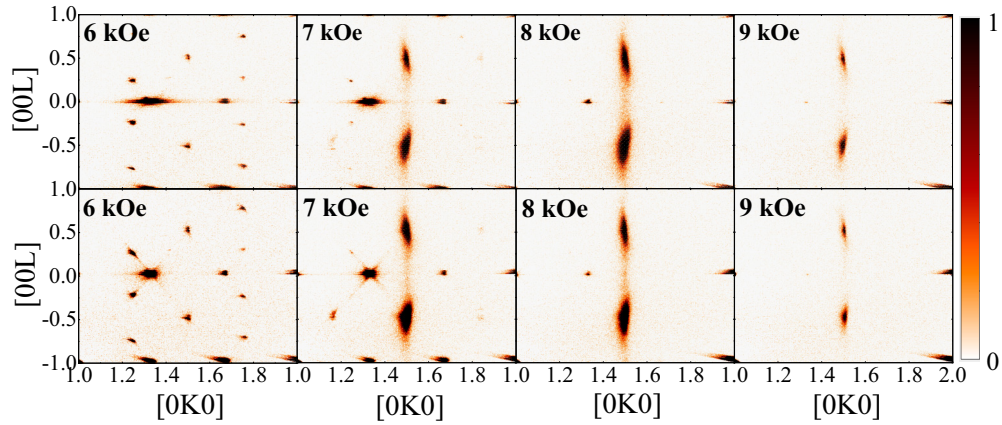

FIG. 8. Development of the magnetic correlations at 0.24 K in D-type $Er_2Si_2O_7$ in a field from 6 to 9 kOe applied along the a axis before (top row) and after exposure to a higher field of 50 kOe (bottom row).

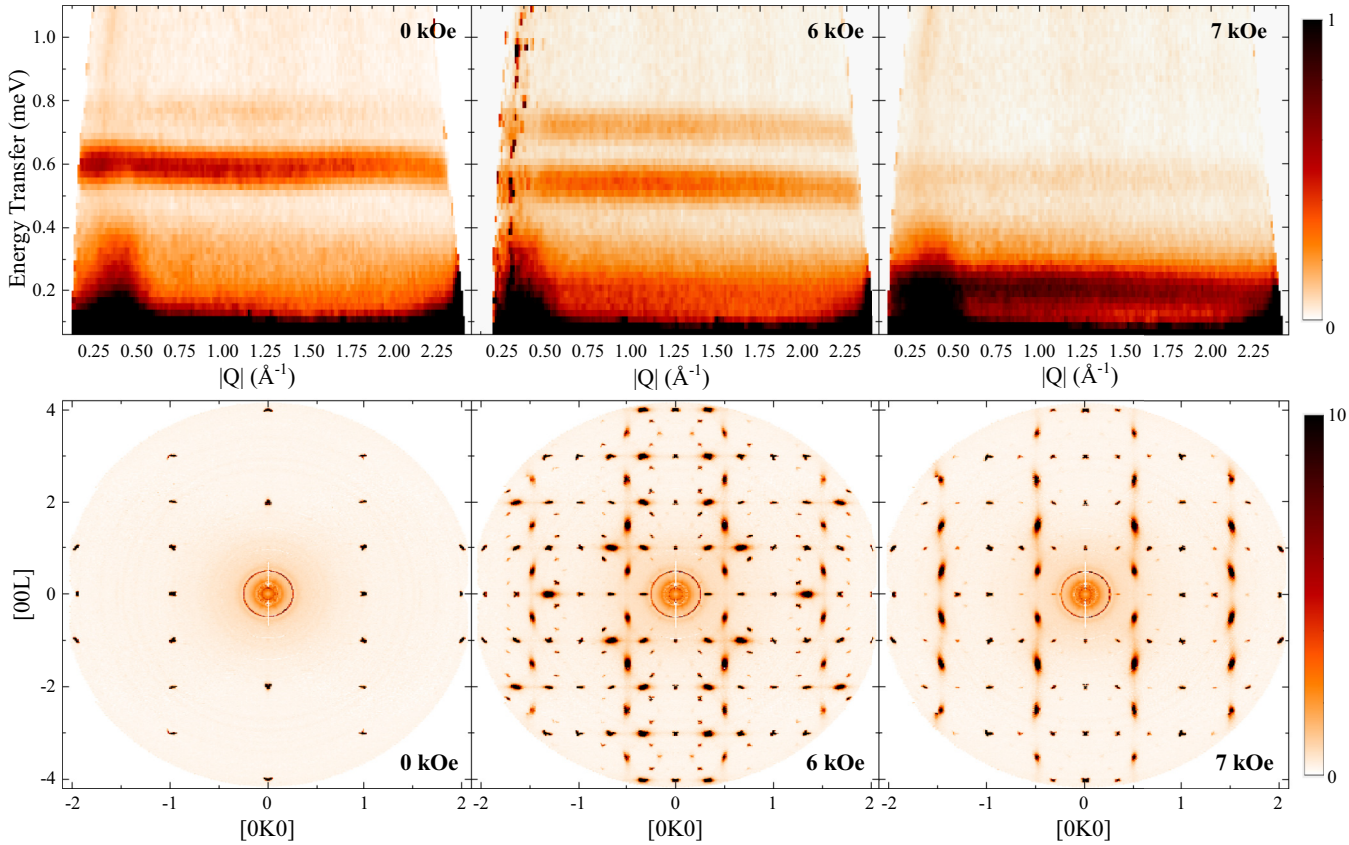

FIG. 9. Top: Evolution of the dynamical structure factor $S(Q, E)$ with field taken on the IN5 spectrometer on a single-crystal sample of D-type $Er_2Si_2O_7$ at $T = 0.045$ K. The resulting energy spectra have been averaged over the rotation of the crystal as only flat, very weakly dispersive excitations are present. The sample was rotated around the a axis ∼43°, parallel to an applied field, H, while the average is taken over the whole detector range. The high-intensity feature at $|Q| = 0.35$ Å^{-1} is an artefact of the cryomagnet and can be ignored. Bottom: Corresponding symmetrized diffraction maps for the zero-energy transfer in the $(0kl)$ plane.

For all the measurements made on IN5, only practically dispersionless excitations were found with no significant dependence of the excitation energy on the scattering vector. We therefore present our measurements as an average over the rotation of the crystal, producing a powder-average spectrum, obtained by grouping the pixellated data of the detector in (|Q|,E) bins, i.e., Debye-Scherrer cones over the entire detector range.

As the orientation of the crystal only allows for measurement of the b^*-c^* plane, this method of averaging cannot represent a true powder-average containing the information for all orientations of the crystals with the incident and scattered neutrons spanning all possible crystal symmetry directions. Our case covers the symmetry directions of interest, in which there is very little dispersion of the inelastic modes. It should be noted, however, that the Q-dependence of the intensity of these excitations cannot be determined. We therefore present the powder-averaged INS data as color-coded intensity maps for different values of the applied field; see Fig. 9.

In zero field, a high-intensity excitation is observed at 0.58 meV, along with a second, lower intensity branch at 0.75 meV, differing from previous powder INS measurements in [9], where two branches were seen at 0.2 and 0.6 meV. With increasing field, the higher intensity branch appears to split into two branches at 0.74 and 0.43 meV in 2 kOe. The energies of the two branches increase and decrease linearly as the applied field is increased further. By 5 kOe, the energy gap between the branches reaches 0.76 meV. The sample enters the plateau phase at 5.5 kOe, confirmed by the presence of the noninteger peaks in the elastic reciprocal space maps. The transition to a plateau regime is accompanied by the appearance of three excitation branches. A full set of the field-dependent excitation spectra can be found in the Supplemental Material [27].

The field dependence of the excitations has been examined via the cuts made along the energy transfer axis in the scattering vector range 1.0–1.5 Å^{-1} [see Fig. 10(a)]. For clarity, the intensity cuts have been plotted separately to follow the excitations both within and outside of the plateau region. The evolution of the excitations with field is plotted in Fig. 10(b), with the area of each point corresponding to the intensity of the excitation branch. The plateau phase is indicated by the dashed lines. While demagnetization effects prevent a direct comparison to our magnetization measurements, the plateau region can be defined via a combination of the elastic diffraction maps accompanying the inelastic powder average spectra and examining the development of the excitations. Although remnants of the noninteger peaks are still present in the elastic diffraction maps for 7–9 kOe, their intensities are greatly reduced. The single, high-energy excitation present in higher fields shown in orange in Fig. 10 is also present from 7 kOe,

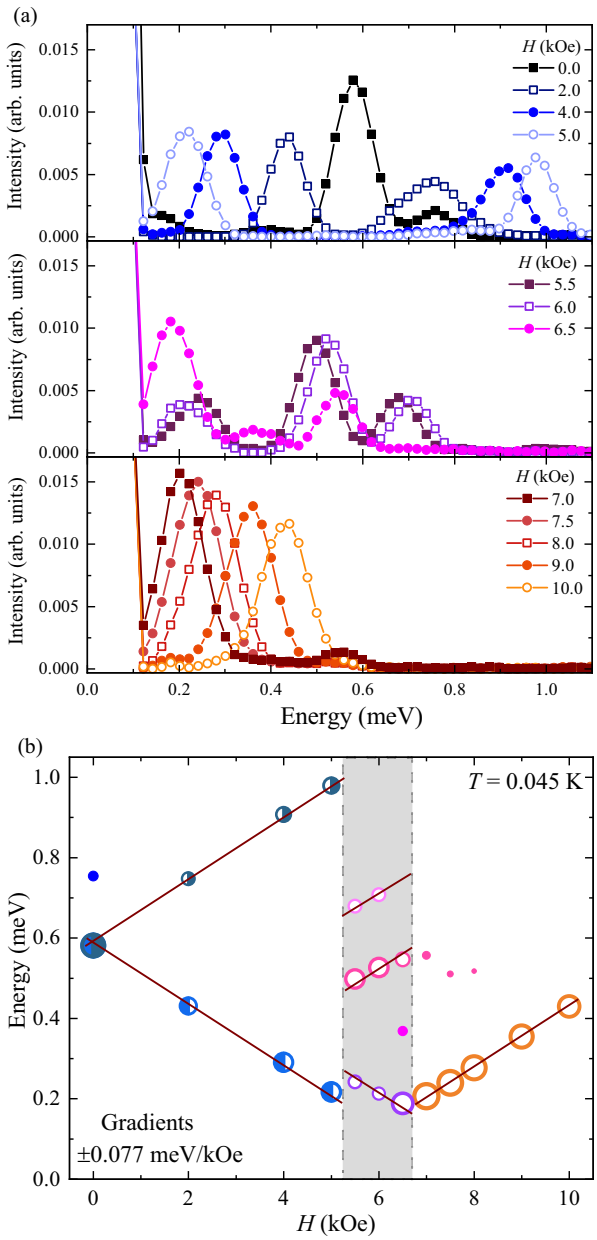

FIG. 10. Field dependence of the excitation energies of $Er_2Si_2O_7$ at $T = 0.045$ K. (a) Cuts along the energy transfer axis of the INS spectra shown in Fig. 9 for $Q = [1.0, 1.5]$ Å^{-1} for different applied fields. (b) The variation of the excitation energies with applied field. The area of the symbols is proportional to the scattering intensity. The vertical dashed lines are guides to the eye and indicate the boundaries between the phases, which we estimate to be at $H_1 \approx 5.2$ kOe and $H_2 \approx 6.7$ kOe. The coloring indicates branches of excitations which follow the variation with the Zeeman energy expected in the three phases: unmagnetized ($H < H_1$), $\frac{1}{3}$-magnetized ($H_1 < H < H_2$), and fully magnetized $H_2 \lesssim H$. The number of main excitations are in line with expectations in both the unmagnetized and fully magnetized phases. The lines through the points are drawn with gradients given by the effective g-factor reported in [8] and assuming the excitation energy varies as $g\mu_B H$, where H is the applied field. We do not expect the magnetization and demagnetizing field to vary significantly in each phase (see the main text).

implying that the system is no longer in the plateau phase and has entered the fully magnetized state.

Distinct field-induced trends can be seen in the excitations below and above the plateau regime. At low fields, the 0.58 meV excitation present in zero field splits into two pronounced branches. The higher-energy branch continues to increase in energy with field while that of the lower-energy excitation decreases with field. The field gradients for increasing and decreasing branches are very similar. This can be rationalized via the spin-flipping mechanism in Ising systems for which the energy of reversing the Ising moments is varying linearly with the applied field. At fields above the plateau, a single high-intensity excitation branch is present. With further field increase, the energy of the excitation increases with the same gradient as the lower-field branch, implying that the system is in the fully magnetized state along the applied field. Remnants of the 0.5 meV excitation, shown in pink in Fig. 10(b), are present immediately above the plateau with a reduced intensity, but they disappear at higher fields.

The system enters the plateau phase above 5 kOe. In this regime, three intense excitation branches are observed, all varying with applied field with the same gradient.

The individual levels of the Er^{3+} ions are Kramers doublets with the energy levels of the ion split by a magnetic field. This splitting is characterized by an anisotropic effective g-tensor. In general, this will be different for different ionic states. Extensive analysis in [8] reported the values of the g-tensor along the principal axes. The Zeeman energy of each of the Ising-like spins was well-approximated by taking $g_z = 13.6$ with $g_x = g_y = 0$, where z is the easy-axis direction of each magnetic ion, and x and y are the two perpendicular directions. For a field varying along the a direction, this would give a Zeeman energy varying as $\pm 0.077\, H$meV, illustrated by the slope of the straight lines in Fig. 10.

IV. MODELING MAGNETIC PROPERTIES

$Er_2Si_2O_7$ is thought to be well described as an Ising-like system. There are two easy magnetization axes set by the crystal fields. Labeling the ions in the unit cell as in Fig. 3(b), ions 1 and 3 share one easy axis and ions 2 and 4 share the other. Our Rietveld refinement gives the total moment as 6.54(4) μ_B with components given in Table I.

The angles of the average magnetization direction $\langle \boldsymbol{m}_a \rangle$ with respect to the a direction and from the ab-plane to the c direction (see Fig. 11) are $\theta = 19.7(4)^\circ$ and $\phi = 18.4(4)^\circ$, respectively. These values differ slightly from previously reported values $\theta = 28^\circ, \phi = 15^\circ$ in [8] and $\theta = 21.3^\circ, \phi = 12.8^\circ$ in [9]. The moment directions quoted in [8] are derived from measurements of the g-tensor using optical spectroscopy and are not directly comparable to the values we find, or those reported in [9], both of which are the results of the refinement of neutron diffraction data. The value we obtain for ϕ fits with a natural explanation of the transitions observed in the magnetization in Fig. 5 and in Fig. 6 as the field increases. The jump to a magnetization of $\sim 2\,\mu_B$ per magnetic ion for fields aligned along the c direction matches the value of 2.08 μ_B of the easy-axis moment resolved along this direction. With

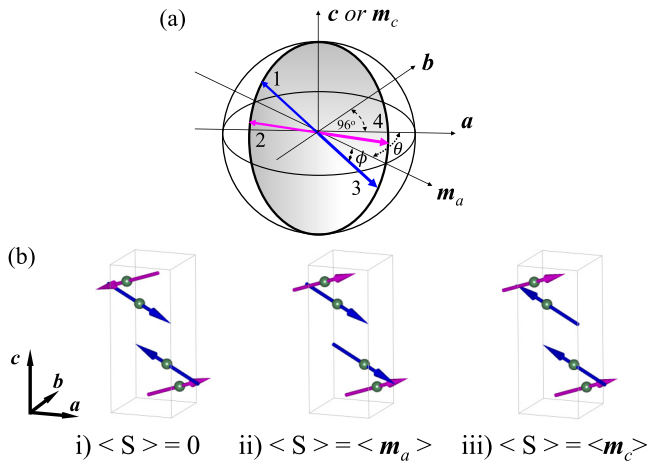

FIG. 11. Configurations of the moments in possible ground states. (a) Perspective view showing the spins 1 and 3 aligned along one easy axis and spins 2 and 4 aligned along the other. This corresponds to the expected ground state in zero applied field. In an applied field we expect spins to flip to maximize their alignment with the field. For a field applied parallel (or near parallel) to $\boldsymbol{a}$, we expect spins 1 and 2 to flip. This gives rise to a net magnetization in the $\langle \boldsymbol{m}_a \rangle$ direction, which is in the plane perpendicular to the c direction at an angle $\theta = 19.7(4)^\circ$ to the a direction. (b) The orientation of the moments in the unit cell: (i) The zero-field case. (ii) The fully magnetized state for a field applied in the a direction. The expected average moment per ion is $\langle \boldsymbol{m}_a \rangle$, which is given in Table I. (iii) The fully magnetised state for a field applied in the c direction.

the field aligned along the a direction, the magnetization rises quickly to $\gtrsim 6\,\mu_B$ as the field is increased from 6.5 to 7.5 kOe. This is close to the moment $6.20(4)\,\mu_B$ from our Rietveld refinement we would expect in the fully magnetized phase. The magnetization in the center of the intermediate phase at 0.5 K, which we estimate as $2.1\,\mu_B$ per Er ion, is close to one-third of the theoretical fully magnetized value.

The interpretation of these transitions, suggested by the model of [8], is that the moments of the ions 1 and 2 reverse direction to align with the magnetic field. The ground-state configuration is assumed to be changing from the one identified as (i) in Fig. 11 to either (ii) or (iii) for the case of a field along the a direction or the c direction. [We have labeled the ions as in Fig. 3(b).] The gradual increase of the moment for increasing fields above the transitions suggests that the easy axis slowly realigns towards the magnetic field with increasing field in both cases. The intermediate phase, with a magnetization of one-third of its expected value in the fully magnetized phase ($6.54\,\mu_B$), requires an enlarged unit cell in which there are two-thirds of a spin flip per original unit cell on average.

The excitations seen in our inelastic data support the validity of an Ising model with two easy axes. In any Ising system, all single-spin flips are eigenstates of the Hamiltonian. Excitations are therefore local and there should be no dispersion of the excitations. As mentioned above, we found close to no dispersion for excitations in our angle-resolved data [27] and presented angle-averaged results in Fig. 9, showing the existence of almost dispersionless bands. In the model of [8], the energies of the possible ground states are characterized by

TABLE II. The parameters giving the contribution to the energy from interactions between an Ising-like spin of an Er ion labeled i in Fig. 3 with all those labeled j in the crystal. (We have used the labeling of ions from [9].) The parameters β, γ, and δ were estimated in [8] from the measured phase diagram, while the parameter α was estimated from spectroscopic measurements. The values quoted were $\alpha = -0.088(6)$ meV, $\beta = 0.015(4)$ meV, $\gamma = -0.144(4)$ meV, and $\delta = -0.050(4)$ meV. (In [8] ion 3 is labeled 4 and vice versa.)

	Ion j, state (i)				Ion j, state (ii)			
Ion i	1	2	3	4	1	2	3	4
1	α	β	δ	γ	α	β	$-\delta$	$-\gamma$
2	β	α	γ	δ	β	α	$-\gamma$	$-\delta$
3	δ	γ	α	β	$-\delta$	$-\gamma$	α	β
4	γ	δ	β	α	$-\gamma$	$-\delta$	β	α

the energy of interaction of the moment i, with all moments of type j in the rest of the lattice. The model assumes that the interactions between ions have the same symmetry as the crystal lattice. For example, ions 1 and 3 share the same easy axis and have the same separations as ions 2 and 4. The interactions between these pairs of ions are taken to be the same, namely δ. On this basis, the contribution to the ground-state energy of a given ion in the unit cell with the other ions in the system in the unit cell is given in Table II.

Assuming that the interactions between Ising spin variables of ions i and j are of the form $J(\boldsymbol{r}_i - \boldsymbol{r}_j)S_iS_j$, where $\boldsymbol{r}_i$ is the position vector of an ion i, the parameters in Table II determine the strength of the local field acting on an individual ion. The energy of an excitation is $\epsilon_\pm(H) = -2(\alpha + \beta + \gamma + \delta) \pm g\mu_B B\cos\psi$ in state (i); see Fig. 11. Here ψ is the angle between the magnetic field and the easy-axis for the spin. We are defining the effective g-factor as in [8], so that the Zeeman energy to flip the Ising effective spin-1/2 is $g\mu_B B\cos\psi$.

In state (i) there are two excitation energies with a splitting given by the Zeeman term. The magnetization is small and the field B is well approximated by the applied field H. In our experiments, the field was applied along the a direction and $\cos\psi = \cos\phi\cos\theta$. With the parameters quoted above and the value given for g (the g-tensor was measured spectroscopically in [8]), the model predicts the excitation energies to be $\epsilon_\pm(H) = 0.53 \pm 0.077\,H$meV, with H in kOe. This agrees remarkably well with the excitation energies shown in Fig. 10 for applied fields $H < H_1 \approx 5.2$ kOe. These have $\epsilon_+ \approx 0.58 + 0.077\,H$ and $\epsilon_- \approx 0.58 - 0.077\,H$meV.

We identify the ground state at applied fields $H > H_2 \approx 6.7$ kOe with spin configuration (ii) characterized in Fig. 11. Here the model also predicts the excitation energy: $\epsilon(H) \approx -2(\alpha + \beta - \gamma - \delta) + g\mu_B H\cos\psi + C$, where C is a constant. The Zeeman energy should vary linearly with the applied field as the magnetization, and hence the demagnetizing field, are expected to be constant within each phase, and their effects are denoted by C. There is only one excitation as any spin must flip against the field. This implies that the excitation energy in meV is $\epsilon(H) \approx -0.24 + g\mu_B H\cos\psi + C$, with H in kOe. The model predicts one dominant excitation. This is close to what we find for the applied fields $H > H_2$ shown in Fig. 10.

In both states (i) and (ii), see Fig. 11, there is evidence for weak scattering by other modes. In state (i) there is some scattering at energy $\epsilon \approx 0.75$ meV, which we observed only in zero field. We do not have an explanation for this within the simple model we are using. In state (ii) there is weak scattering at $\epsilon \sim 0.5$ meV, which disappears at higher fields. Again, we cannot explain this within the model.

The magnetic field in the sample will be significantly different from the applied field once the system magnetizes. This is because the magnetization is not parallel to the applied field and because of demagnetizing effects. For applied fields $H \lesssim 10$ kOe, the magnetization is close to one of three values: 0, $\langle \boldsymbol{m}_a \rangle/3$, and $\langle \boldsymbol{m}_a \rangle$. The demagnetizing effects are hard to quantify, but are apparent in our results. For example, the magnetization results shown in Fig. 5 (inset) show that the transition into the fully magnetized phase occurs at an applied field $H \sim 6.5$ kOe at 0.50 K. The same transition appears at the slightly higher applied field $H_2 \sim 6.7$ kOe in the sample studied via inelastic neutron scattering; see Fig 10 (where data were taken at the temperature of 0.045 K). The samples in these two measurements were different so that direct mapping between applied fields for the magnetization and neutron scattering measurements is not possible on account of the demagnetizing effects.

In the case of the sample studied by inelastic neutron scattering, its shape was approximately a half-cylinder. The axis of the cylinder was 27° away from the *a* axis in the *ac* plane. None of the applied field, the magnetization direction $\langle \boldsymbol{m}_a \rangle$, and the demagnetizing field would be aligned with the cylinder axes. For some directions of applied field, the resultant field has different projections along the two easy axes, which would lead to a further splitting of the Zeeman split excitations. For the particular case of the field applied parallel to the *a* axis, our estimates suggest that this splitting is negligible. (We assumed a uniform demagnetizing tensor with component $0.15 \times 4\pi$ along the axis and equal components in the perpendicular directions.)

The identification of the intermediate phase is difficult. We would like to establish for which directions of applied field the phase exists (we have only looked along one direction) as well as find the new ordered state. The diffraction data shown in Figs. 7 and 8 indicate possible Bragg as well as diffuse peaks corresponding to propagation vectors $\mathbf{q} = [0\tfrac{1}{3}0]$ and $[0\tfrac{1}{4}\tfrac{1}{4}]$. The nature of the phase also seems to vary with applied field. Within the easy-axis model, the magnetization and diffraction data imply a state with enlarged periodicity in both *b* and *c* directions and with an average of two-thirds of a spin-flip per each original unit cell. It might be possible to explain the magnetization with an enlarged cell, for example 4×4 but not involving a factor 3, and flipping close to two-thirds of a spin per original unit cell. However, this would make it difficult to explain the scattering corresponding to propagation vectors $\mathbf{q} = [0\tfrac{1}{3}0]$.

Our model assumes that the magnetization and, hence, the demagnetizing field are constant in each phase including the intermediate phase. We therefore expect only the applied component of the total field to be varying. The variation of the excitation energies with applied field would then still show the linear dependence of the Zeeman energy seen in the unmagnetized and fully magnetized cases. This is close to what we see. The small deviation from this behavior, slightly below the transition at $H = H_2$ (see Fig. 10), may also be connected with the variation of the phase seen in the diffraction data.

V. SUMMARY

Magnetic measurements and a range of neutron scattering techniques have been employed to investigate the in-field behavior of D-type $Er_2Si_2O_7$, an Ising-like antiferromagnet. PND data confirm the formation of a four-sublattice $\mathbf{q} = \mathbf{0}$ structure below the ordering temperature of $T_N = 1.85$ K with two pairs of collinear antiferromagnetic moments within the crystallographic unit cell. Magnetization measurements with the field applied along the *a* axis of a single crystal of $Er_2Si_2O_7$ reveal the existence of a narrow and temperature-sensitive magnetization plateau at $\frac{1}{3}$ of the saturation magnetization. In-field single-crystal neutron diffraction has shown that the magnetic unit cell undergoes a significant increase within the plateau regime demonstrated by the appearance of a scattering signal at noninteger positions described by the propagation vectors $\mathbf{q} = (0\tfrac{1}{2}\tfrac{1}{2})$, $\mathbf{q} = (0\tfrac{1}{4}\tfrac{1}{4})$, and $\mathbf{q} = (0\tfrac{1}{3}0)$. The intensity, shape, and width of these field-induced features change rapidly with the applied magnetic field within the magnetization plateau. The diffraction pattern then returns to integer peaks at higher fields, upon its entrance into the paramagnetic phase and out of the plateau.

Inelastic neutron scattering data indicate flat, almost dispersionless excitations, as expected in an Ising-like system. Below the plateau, two intense excitation branches are observed, one linearly increasing with field and the other decreasing while above the plateau; only one branch is visible. The field gradients for all three branches are well described by the previously determined *g*-factor for the Er^{3+} magnetic ions. Within the plateau regime, the excitation spectrum corresponds to an increased magnetic unit cell and contains three intense branches. This observation should restrict the number of candidate ground states significantly. Enlarging the magnetic unit cell leads quickly to an increase in the number of inequivalent spin flips and hence the number of excitations, while our data show only three significant excitations.

ACKNOWLEDGMENTS

We acknowledge the technical support and expertise of the sample environment teams at ISIS and ILL. The work at the University of Warwick was supported by EPSRC through Grants No. EP/M028771/1 and No. EP/T005963/1.

[1] J. Ito and H. Johnson, Synthesis and study of yttrialite, Am. Mineral. **53**, 1940 (1968).

[2] J. Felsche, Polymorphism and crystal data of rare-earth disilicates of type $RE_2Si_2O_7$, J. Less-Common Met. **21**, 1 (1970).

[3] A. Maqsood, B. Wanklyn, and G. Garton, Flux growth of polymorphic rare-earth disilicates, $R_2Si_2O_7$ (R = Tm, Er, Ho, Dy), J. Cryst. Growth **46**, 671 (1979).

[4] A. Kitaev, Anyons in an exactly solved model and beyond, Ann. Phys. **321**, 2 (2006).

[5] G. Hester, H. S. Nair, T. Reeder, D. R. Yahne, T. N. DeLazzer, L. Berges, D. Ziat, J. R. Neilson, A. A. Aczel, G. Sala, J. A. Quilliam, and K. A. Ross, Novel strongly spin-orbit coupled quantum dimer magnet: Yb_2 Si_2 O_7, Phys. Rev. Lett. **123**, 027201 (2019).

[6] G. Hester, T. N. DeLazzer, S. S. Lim, C. M. Brown, and K. A. Ross, Néel ordering in the distorted honeycomb pyrosilicate: C − $Er_2Si_2O_7$, J. Phys.: Condens. Matter **33**, 125804 (2021).

[7] M. C. Hatnean, O. A. Petrenko, M. R. Lees, T. E. Orton, and G. Balakrishnan, Optical floating zone crystal growth of rare-earth disilicates, $R_2Si_2O_7$ (R = Er, Ho, and Tm), Cryst. Growth Des. **20**, 6636 (2020).

[8] M. J. M. Leask, P. R. Tapster, and M. R. Wells, Magnetic properties of D-type $Er_2Si_2O_7$, J. Phys. C **19**, 1173 (1986).

[9] G. Hester, T. N. DeLazzer, D. R. Yahne, C. L. Sarkis, H. D. Zhao, J. A. R. Rivera, S. Calder, and K. A. Ross, Magnetic properties of the ising-like rare earth pyrosilicate: D-$Er_2Si_2O_7$, J. Phys.: Condens. Matter **33**, 405801 (2021).

[10] A. Okutani, T. Kida, Y. Narumi, T. Shimokawa, Z. Honda, K. Kindo, T. Nakano, Y. Nozue, and M. Hagiwara, High-field magnetism of the honeycomb-lattice antiferromagnet $Cu_2(pymca)_3(ClO_4)$, J. Phys. Soc. Jpn. **88**, 013703 (2019).

[11] M. Adhikary, A. Ralko, and B. Kumar, Quantum paramagnetism and magnetization plateaus in a kagome-honeycomb Heisenberg antiferromagnet, Phys. Rev. B **104**, 094416 (2021).

[12] H. Ninomiya, Y. Matsumoto, S. Nakamura, Y. Kono, S. Kittaka, T. Sakakibara, K. Inoue, and S. Ohara, Magnetic properties and magnetic phase diagrams of trigonal $DyNi_3Ga_9$, J. Phys. Soc. Jpn. **86**, 124704 (2017).

[13] F. A. G. Albarracín and H. D. Rosales, Multiple pseudo-plateaux states and antiferromagnetic pair selection in the XY model in the highly frustrated honeycomb lattice, J. Phys.: Condens. Matter **33**, 185801 (2021).

[14] H. S. Nair, T. DeLazzer, T. Reeder, A. Sikorski, G. Hester, and K. A. Ross, Crystal growth of quantum magnets in the rare-earth pyrosilicate family $R_2Si_2O_7$ (R = Yb, Er) using the optical floating zone method, Crystals **9**, 196 (2019).

[15] N. Shirakawa, H. Horinouchi, and Y. Yoshida, Measuring Sr_2RuO_4 down to 0.5K with a commercial SQUID magnetometer combined with ^{3}He refrigeration, J. Magn. Magn. Mater. **272-276**, E149 (2004).

[16] A. Aharoni, Demagnetizing factors for rectangular ferromagnetic prisms, J. Appl. Phys. **83**, 3432 (1998).

[17] L. C. Chapon, P. Manuel, P. G. Radaelli, C. Benson, L. Perrott, S. Ansell, N. Rhodes, D. Raspino, D. Duxbury, E. Spill, and J. Norris, Wish: The new powder and single crystal magnetic diffractometer on the second target station, Neutron News **22**, 22 (2011).

[18] O. A. Petrenko, G. Balakrishnan, M. C. Hatnean, and P. Manuel, Magnetic order in $Er_2Si_2O_7$, STFC ISIS Neutron and Muon Source, doi: 10.5286/ISIS.E.RB1910545.

[19] J. Rodríguez-Carvajal, Recent advances in magnetic structure determination by neutron powder diffraction, Phys. B: Condens. Matter **192**, 55 (1993).

[20] O. A. Petrenko, G. Balakrishnan, M. Ciomaga Hatnean, M. Islam, and J. Ollivier, Field-induced phases and magnetisation plateau in $Er_2Si_2O_7$, Institut Laue-Langevin (ILL), doi: 10.5291/ILL-DATA.4-01-1697.

[21] J. Ollivier and H. Mutka, IN5 cold neutron time-of-flight spectrometer prepared to tackle single crystal spetroscopy, J. Phys. Soc. Jpn. **80**, SB003 (2011).

[22] O. Arnold, J. C. Bilheux, J. M. Borreguero, A. Buts, S. I. Campbell, L. Chapon, M. Doucet, N. Draper, R. F. Leal, M. A. Gigg, V. E. Lynch, A. Markvardsen, D. J. Mikkelson, R. L. Mikkelson, R. Miller, K. Palmen, P. Parker, G. Passos, T. G. Perring, P. F. Peterson *et al.*, Mantid Data analysis and visualization package for neutron scattering and μ SR experiments, Nucl. Instrum. Methods Phys. Res., Sect. A **764**, 156 (2014).

[23] R. A. Ewings, A. Buts, M. D. Le, J. van Duijn, I. Bustinduy, and T. G. Perring, HORACE: Software for the analysis of data from single crystal spectroscopy experiments at time-of-flight neutron instruments, Nucl. Instrum. Methods Phys. Res., Sect. A **834**, 132 (2016).

[24] Y. A. Izyumov, V. E. Naish, and R. P. Ozerov, in *Neutron Diffraction of Magnetic Materials* (Springer, Boston, 1991), pp. 137–222.

[25] H. T. Stokes, D. M. Hatch, and B. J. Campbell, ISODISTORT, ISOTROPY Software Suite, iso.byu.edu.

[26] B. J. Campbell, H. T. Stokes, D. E. Tanner, and D. M. Hatch, ISODISPLACE: A web-based tool for exploring structural distortions, J. Appl. Crystallogr. **39**, 607 (2006).

[27] See Supplemental Material at http://link.aps.org/supplemental/10.1103/PhysRevB.109.094420 for a full set of $Er_2Si_2O_7$ data.

[28] O. Young, A. R. Wildes, P. Manuel, B. Ouladdiaf, D. D. Khalyavin, G. Balakrishnan, and O. A. Petrenko, Highly frustrated magnetism in $SrHo_2O_4$: Coexistence of two types of short-range order, Phys. Rev. B **88**, 024411 (2013).

[29] T. J. Hayes, G. Balakrishnan, P. P. Deen, P. Manuel, L. C. Chapon, and O. A. Petrenko, Coexistence of the long-range and short-range magnetic order components in $SrEr_2O_4$, Phys. Rev. B **84**, 174435 (2011).